ACTUATORS

3D-printed biomimetic artificial muscles using soft actuators that contract and elongate

Corrado De Pascali[1,2]*, Giovanna Adele Naselli[1]†, Stefano Palagi[1,2]†, Rob B. N. Scharff[1], Barbara Mazzolai[1]*

Biomimetic machines able to integrate with natural and social environments will find ubiquitous applications, from biodiversity conservation to elderly daily care. Although artificial actuators have reached the contraction performances of muscles, the versatility and grace of the movements realized by the complex arrangements of muscles remain largely unmatched. Here, we present a class of pneumatic artificial muscles, named GeometRy-based Actuators that Contract and Elongate (GRACE). The GRACEs consist of a single-material pleated membrane and do not need any strain-limiting elements. They can contract and extend by design, as described by a mathematical model, and can be realized at different dimensional scales and with different materials and mechanical performances, enabling a wide range of lifelike movements. The GRACEs can be fabricated through low-cost additive manufacturing and even built directly within functional devices, such as a pneumatic artificial hand that is fully three-dimensionally printed in one step. This makes the prototyping and fabrication of pneumatic artificial muscle–based devices faster and more straightforward.

INTRODUCTION

All muscles in the animal kingdom consist of bundles of uniaxially contractile fibers, in turn made of identical sarcomere units, yet muscles are not at all equal. They have sizes spanning three orders of magnitude (from meters down to millimeters), a variety of shapes and architectures (spatial distributions of fibers within the muscle), and complex arrangements within the body (including antagonistic pairs), enabling the dexterity and wide ranges of movement amplitudes, speeds, and forces observed in animals (1, 2). Muscles represent, therefore, a reference for actuators in artificial machines, not only because of their remarkable performances in terms of force, power, and durability [which have been met and even surpassed (3, 4)] but especially for their astonishing versatility that is still largely unmatched (Fig. 1A) (5–8).

Actuators that are designed to perform muscle-like contraction are known as artificial muscles (9, 10). Pneumatic artificial muscles (PAMs), which contract upon pressurization, were first introduced in the 1950s and usually consist of a flexible or stretchable cylindrical membrane that is constrained by high tensile-resistant fibers and capped by two rigid end fittings (11–14). The fibers and fittings are needed because they translate the membrane's volume increase (and consequent radial expansion) into a longitudinal contraction (15–19). Starting from the traditional PAMs, pneumatics have widely spread in soft robotics, particularly to reproduce the muscle's contraction in bioinspired robots (20, 21). Within the soft robotics field, numerous pneumatic actuators were developed, becoming lighter and less expensive (22), achieving multiple possible deformations (23), improving their compactness (24), or markedly reducing their radial size (25, 26). Despite these recent results, the layout of PAMs still involves a number of assembled components, inherently hindering miniaturization, implementation of non–fusiform-like architectures (required for complex lifelike movements), and the

wide adoption and customization of artificial muscle technologies (27). Therefore, radically simpler PAM designs are needed that are amenable to dimensional scaling, customization to specific needs, and fabrication by accessible additive manufacturing techniques (Fig. 1B) (28–30). These will contribute to democratizing artificial muscles' applications and will allow artificial machines to move with grace and dexterity akin to those of animals and humans.

Here, we propose a class of PAMs made of just one monolithic element: a membrane with an engineered shape. The membrane geometry inherently implements the coupling of inflation to axial contraction, with no need for tensile-resistant components, end caps, or constraints (Fig. 1C). We moved from the concept of pleat-guided deformation, partially exploited also in a traditional class of PAMs named Pleated PAMs (31, 32). Here, however, we iteratively designed and prototyped pleated membrane structures to achieve muscle-like axial contraction upon pressurization-driven unfolding of the pleats—with no need for strain-limiting elements or end caps. The obtained general parametric geometry represents the starting point for designing actuators that contract and/or elongate, inherently enabling antagonistic operation. For this reason, we named our artificial muscles GeometRy-based Actuators that Contract and Elongate (GRACE; Movie 1).

RESULTS

Here, we show that the GRACEs are highly effective, yet convenient and extremely versatile artificial muscles. They exhibit strokes above 30%, with load/weight ratios from hundreds up to over thousands (depending on the membrane material; Fig. 2, A and B, and movie S1). Moreover, they can maximize contraction, elongation, or antagonistic actuation by design, and they can be fabricated in different materials (fig. S4), with different low-cost three-dimensional (3D) printers and at various scales (Fig. 2C and movie S2). Last, they can be seamlessly built-in in complex devices enabling sophisticated and diverse movements.

All these features are enabled by the GRACEs' operating function: a low-strain geometrical transformation of the actuators'

[1]Bioinspired Soft Robotics Laboratory, Istituto Italiano di Tecnologia, Genoa, Italy.
[2]BioRobotics Institute, Scuola Superiore Sant'Anna, Pontedera, Italy.
*Corresponding author. Email: corrado.depascali@iit.it (C.D.P.); barbara.mazzolai@iit.it (B.M.)
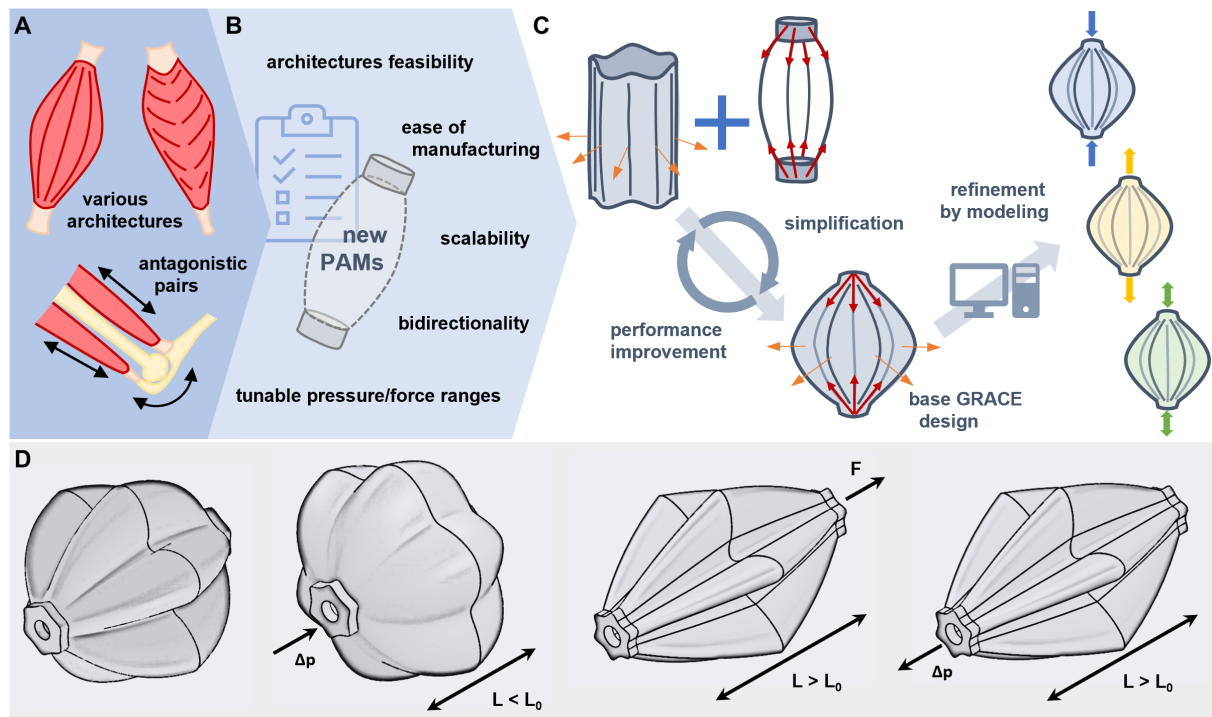†These authors contributed equally to this work.

Fig. 1. GRACE artificial muscles concept. (**A**) Skeletal muscles vary widely in size, architecture, and performance and are inherently suited to antagonistic operation. (**B**) Analogously, we aimed at developing PAMs that are easy to manufacture and to use in complex architectures, scalable, bidirectional and thus well suited for antagonistic operation. Moreover, the envisioned PAMs should have tunable input pressure and output force. (**C**) We developed a base design that intrinsically couples radial expansion and axial contraction in a single monolithic pleated membrane (without the need for strain-constraining elements). By further refining this design, we developed a number of different actuators with different behaviors and performance. (**D**) The operating functions of the GRACEs include contraction and passive and active elongation.
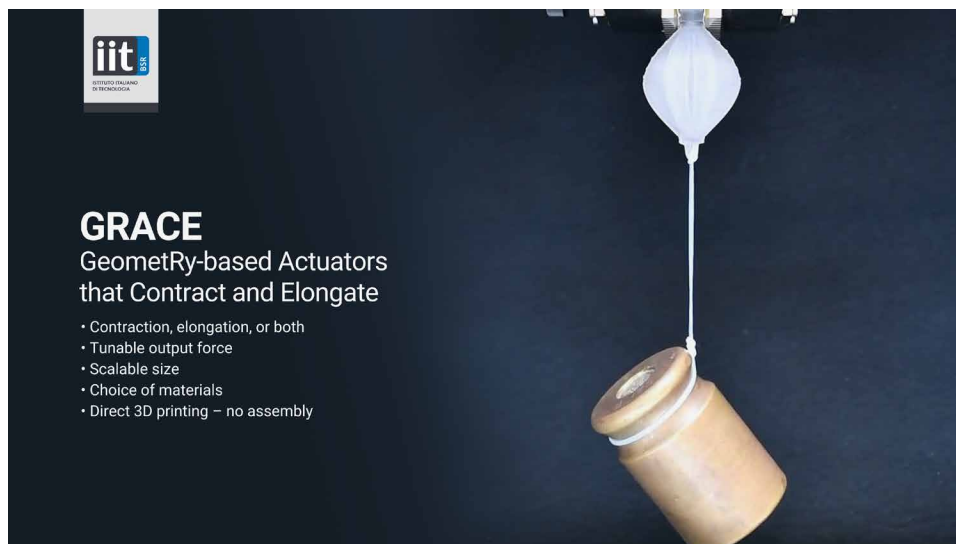
Movie 1. Overview of the GRACE artificial muscles.

structure. The GRACEs consist of a thin shell having a curvilinear shape, narrowing at the two extremities, and longitudinal engineered pleats. When pressurized, the actuator expands radially as the pleats unfold circumferentially (with no substantial stretch of the membrane), and the two extremities are brought together to the middle resulting in a longitudinal contraction (Fig. 1D). In contrast, upon depressurization, the pleats fold, leading to radial contraction and consequent longitudinal elongation (Fig. 1D). Unlike in the so-called Pleated PAMs (*31, 32*),

here the pleats are shaped to inherently enable the contraction and/or elongation of the monolithic GRACEs, with no need for constraining components such as high-tensile resistant fibers or rigid end caps. In the GRACEs, the curvilinear profiles of the pleats and the overall actuator's shape are key, whereas in the Pleated PAMs, the pleats only played a secondary role in the actuation (they eased the circumferential expansion of the actuator's inner membrane, reducing the membrane stretch compared with the conventional McKibben's design, though without altering the contraction function that similarly relied on tensile-resistant fibers).

Geometrical modeling

As shown in fig. S1A, the central cross section of a GRACE consists of a closed series of elliptical arcs whose concavity alternates to generate the pleats. The GRACE surface results from smoothly transitioning (lofting) such cross section along longitudinal parabolic curves (fig. S1B) up to the end section on both sides. We compute the deformed configuration of the GRACE as the configuration at which its enclosed volume (fig. S1C) is maximum (or minimum) in case of contraction (or extension). Our approach is purely geometrical, because the lengths of all the parabolic and elliptical arcs are required to

Fig. 2. GRACE muscles with tunable force output and scalable size. (**A**) A 4-cm-long, 6-g GRACE made of Flexible 80A resin by Formlabs (SLA) lifts up a 1-kg load with a contraction of 20% lengthwise. (**B**) A 4-cm-long, 8-g GRACE made of Flexfill TPU 98A by Fillamentum (FDM) lifts up a 8-kg load with a contraction of 20% lengthwise. (**C**) GRACEs of sizes spanning one order of magnitude.

However, this is a coarse simplification, and understanding the role played by each geometrical parameter is not trivial (see Supplementary Methods).

Finite element analysis

On the basis of the parameters obtained for the three versions of the GRACEs (table S1) and setting the desired length (40 mm for most actuators), we defined their actual designs, identifying suitable wall thickness and material through finite element analysis (FEA; Fig. 3D and fig. S4). We thus simulated the force exerted by the actuators, as well as the membrane stress and strain distributions, at given input pressures for different thicknesses and material elastic moduli. Starting from a homogeneous thickness of 1 mm (convenient for our intended manufacturing technology), we found that materials with an elastic modulus of about 5 MPa would ensure the desired contraction/elongation and considerable forces (in the order of tens of newtons) at conveniently low pressures (in the order of tenths of bars). We thus simulated actuators made with a material having properties in this range (Formlabs Flexible 80A) and locally refined the walls thickness to reduce stress concentrations (Fig. 3D). Simulating free contraction and elongation conditions (contraction and elongation without constraints or loads applied), we found contractions and elongations that are slightly smaller and larger, respectively, than those predicted by the model and maximum local strains below 30% (fig. S5) for all considered versions of the GRACEs. The simulations indicate that the operating pressure ranges and resulting output forces of the GRACEs can be increased by simply using stiffer materials and/or making the membrane thicker (see Supplementary Methods).

Characterization of actuation performance

We directly printed the different GRACEs by low-cost desktop 3D printers and commercial materials (Form 2 printer and Flexible 80A resin by Formlabs; Fig. 3E). We first characterized the GRACEs by tensile tests (stretching, fig. S6D). GRACE-A exhibits the lowest initial tensile stiffness (about half of that of GRACE-C and comparable to that of GRACE-E), which allows it to be easily stretched by the contraction of an antagonistic muscle. This confirms what we observed in simulations (see Supplementary Methods and fig. S6): GRACE-As are better suited for antagonistic operation (especially at low pressures/deformations) than the other designs. This advantage is further enhanced by the possibility of assisting the contraction of a muscle by extending its antagonist actively (through depressurization).

We then investigated the contraction (+20 kPa) and extension (−10 kPa) of the different GRACEs by isotonic (constant force) and
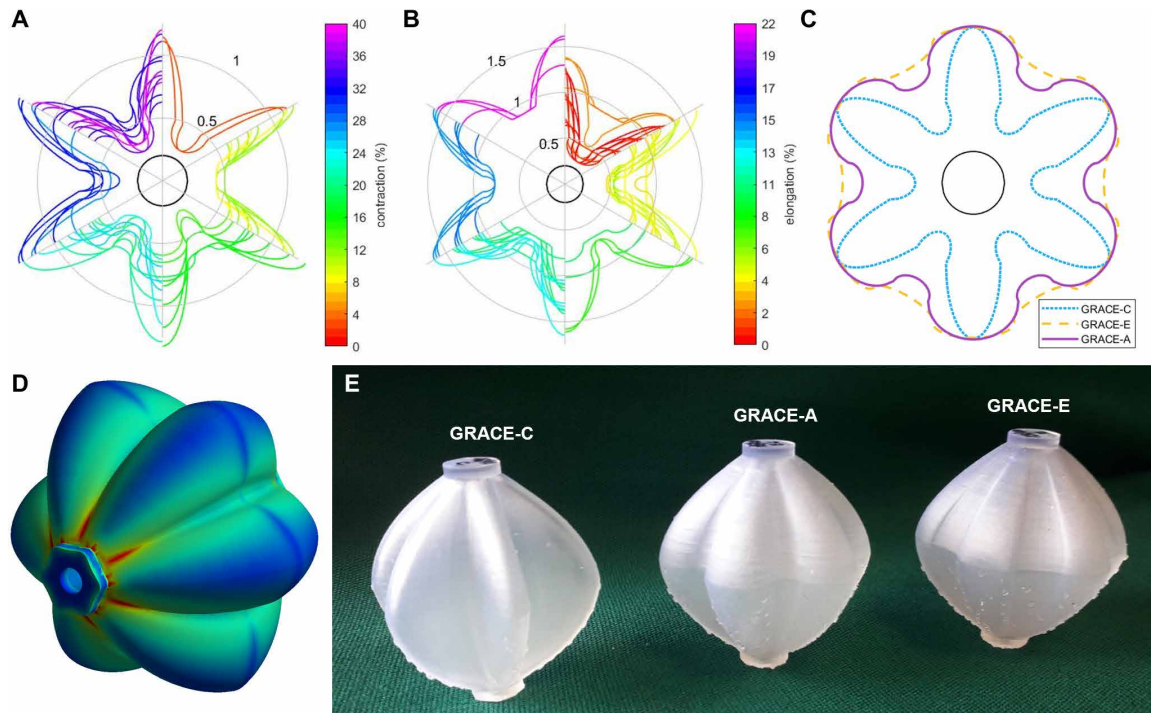
remain unchanged under actuation. In other words, we treated the GRACE as an inextensible membrane with null thickness. Normalization of all lengths ensures that the results are valid at any scale.

We used our model to investigate how the shape of the pleats influences the GRACE's behavior. The model allows to consider any number of pleats. Here, for brevity, we discuss the results obtained for 40,320 different GRACE designs with six pleats, having computed their maximum contraction (Fig. 3A) and elongation (Fig 3B). The profiles that perform better in contraction are those with narrow ellipses and deep pleats, which can largely expand when the GRACE is inflated (we will denote this design by GRACE-C). On the contrary, if actuators that perform deflation-driven elongation are desired, the required GRACE designs are characterized by shallow pleats (GRACE-E). If, instead, actuators are needed that perform best in antagonistic configuration, a suitable geometry is found that performs well both in elongation and in contraction (GRACE-A). Figure 3C shows the central cross section of the three obtained GRACE versions, highlighting that the GRACE-A profile lies between the GRACE-C and the GRACE-E. The same process can be followed to find optimal geometries for a different number of pleats (see Supplementary Methods). Generally, the same considerations hold: narrow and deep pleats promote the contraction, whereas the extension is enabled by wider and more shallow pleats.

Fig. 3. GRACE multiparametric model. (**A**) Contraction and (**B**) elongation (as percentage of initial length) for different profiles. (**C**) Central cross section of GRACE-C (maximizing Contraction), GRACE-E (maximizing Elongation), and GRACE-A (maximizing bidirectional actuation, best suited for Antagonistic operation). (**D**) Maximum principal stress distributions for GRACE-C muscle during isometric contraction resulting from the FEA. (**E**) 3D-printed samples of the three GRACE designs.

isometric (constant length) tests. In the isotonic tests (movie S3), we applied and held three different tensile loads (0 N—free actuation, 4 N, and 8 N) while subjecting the actuators to five pressurization cycles and measuring their contraction and elongation (see Supplementary Methods). GRACE-C samples performed about 25% free contraction and showed decreasing shortening at increasing loads (Fig. 4, A and B, and fig. S7). In contrast, the shortening of GRACE-A samples increased with increasing loads, up to 17.5% with 8 N (fig. S9). As the load stretches the actuators, the pleats fold slightly, thus increasing the unfolding range. The GRACE-A samples also showed about 20% free extension (just slightly lower than that of the GRACE-Es) and elongation decreasing with increasing load (fig. S11). Overall, GRACE-As exhibit an actuation range (contraction and elongation) of 25 to 30% (Fig. 4C), slightly higher than the contraction of GRACE-Cs. In the isometric tests (movie S4), we applied and held three different values of fixed stretch (0 mm—blocking force, 4 mm, and 8 mm), while applying five pressurization cycles and measuring the output forces. The GRACE-C samples exerted a blocking force of 17 N and a maximum pulling force of about 18 N with a 4-mm stretch (Fig. 4, D and E, and fig. S8). In contraction, the GRACE-A samples performed a blocking force of about 7 N and pulling forces increasing with the applied stretch up to about 14 N (fig. S10). In extension, they achieved a 7.5 N blocking force and a pushing force peaking to 9.5 N with the 4-mm stretch (fig. S12).

Compared with skeletal muscles, the GRACEs we tested here exhibit similar deformations and lower forces. The shortening of GRACE-Cs is comparable to the typical values for muscles (about 20%), whereas the actuation range of GRACE-As approaches the maximum range achievable by muscles (>40%) (3, 4). Both GRACE-C and GRACE-A samples showed contraction forces lower than the

ones typically exerted by muscles of equivalent diameter (about 10^2 N; Fig. 4F) (3, 4), yet these can be achieved by GRACEs fabricated with stiffer materials and a thicker membrane and actuated with higher pressures (see fig. S4 and movie S1). Therefore, force performance is limited by the specific material we used in the characterization, not by the GRACE design.

The adopted material (Flexible 80A resin by Formlabs), however, is advantageous in studying the GRACEs because it is inherently photoelastic (its optical properties change in response to local stresses). Through a plane polariscope setup, we captured the stress-induced fringe patterns during both isometric and isotonic actuation (Fig. 4, G and H, and movie S5). The outcomes allowed us to visualize that the stereolithography (SLA) process did not generate any substantial residual stress in the fabricated structures and to collect feedback on the results from FEA, improving the design. The observed color patterns qualitatively match the stress distributions from the FEA, showing a stress concentration in the inward pleats near the two extremities, which led us to preemptively refine the membrane thickness locally to avoid premature failure of the actuators.

We then tested our 3D-printed actuators for 1000 cycles of free contraction or extension (Fig. 4I and fig. S16). GRACE-C consistently reached 26% contraction (compared with initial length), and GRACE-A consistently achieved 12% contraction and about 20% elongation. No failure or permanent changes were observed during the tests, suggesting that even when fabricated with a low-cost desktop 3D printer and a commercial material, the GRACEs can easily withstand many actuation cycles. We also tested the GRACE-C for 20 actuation cycles with input frequencies spanning from 0.066 to 1 Hz to examine its dynamical behavior (fig. S15), which, nonetheless, strongly depends on the whole pneumatic driving system.
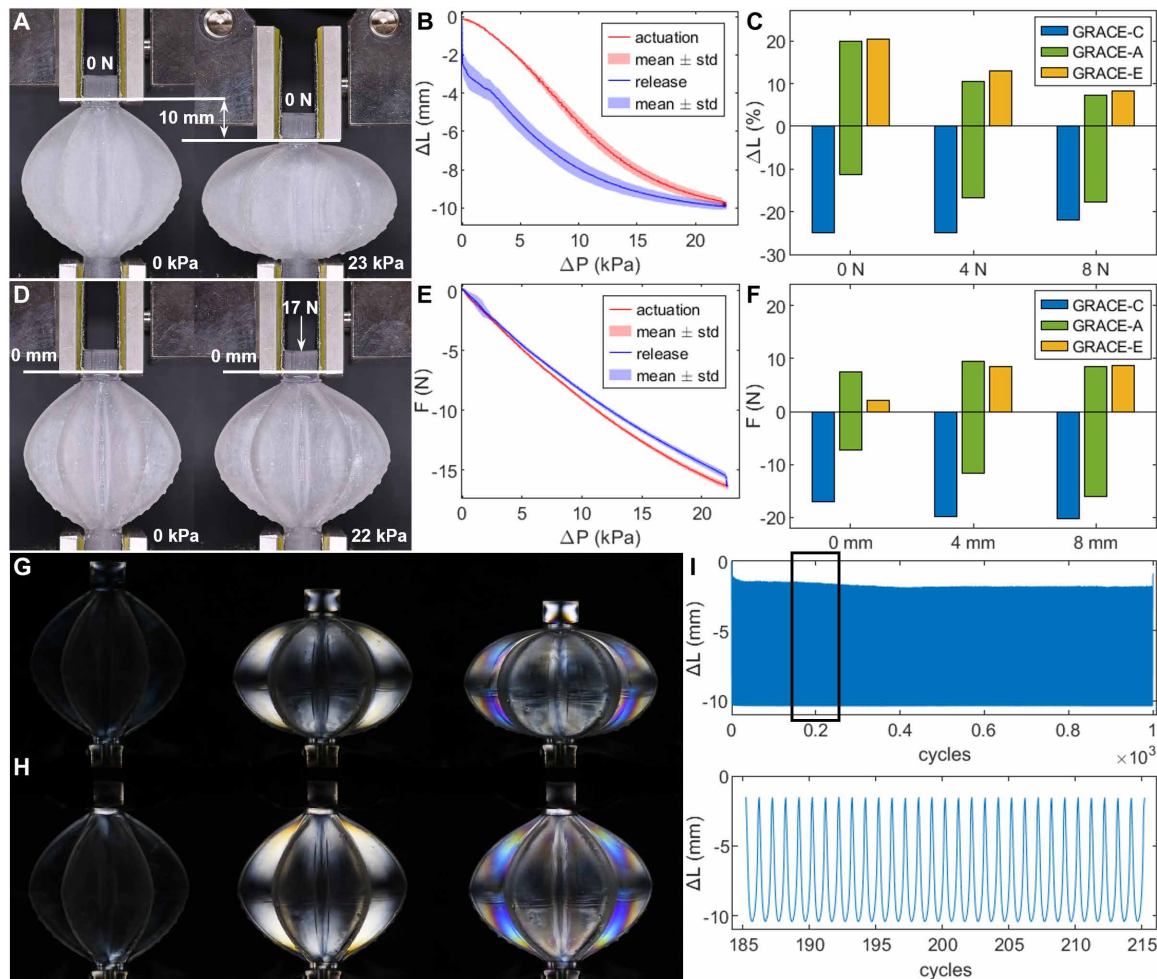
Fig. 4. GRACE muscles' characterization and durability. GRACE-C no-load isotonic tests: (**A**) rest state (left) and inflated state (right); (**B**) actuation (inflation) and release (deflation) curves (mean over five cycles and five samples). (**C**) Shortening/elongation of the three designs in isotonic tests at different loads. GRACE-C no-stretch isometric tests: (**D**) rest (left) and inflated (right) states; (**E**) actuation and release curves (mean over five cycles and five samples). (**F**) Pulling/pushing force of the three designs in isometric tests at different stretches. Stress distribution in GRACE-Cs revealed by photoelasticity during a no-load isotonic test (**G**) and a no-stretch isometric test (**H**). (**I**) No-load cycling of a GRACE-C: The initial length is not recovered within the relaxation phase of the cycles (15 s, overpressure linearly ramping down to zero), most likely because of the material's viscoelasticity, yet it is recovered at the end of the test.

GRACE-based "robotic hand"

Although they exhibit performance on par with state-of-the-art PAMs (table S3), the distinguishing feature of the GRACEs is their extreme versatility. To showcase some of their versatility, we 3D-printed a full GRACE-based pneumatic robotic hand that consists of a palm, five fingers with built-in tendons and flexible joints, and a mobile wrist. We developed this pneumatic robotic hand to show the wide variety of smooth movements that can be achieved by incorporating GRACEs either in series, in parallel, in antagonistic configurations, of different sizes, or directly embedded in a complex functional structure. The full hand has dimensions of 180 mm height by 160 mm width by 50 mm thickness. The hand was directly 3D-printed as a single-material monolithic structure, without requiring assembly and ready for pneumatic actuation (Fig. 5E and fig. S19), demonstrating that the GRACEs enable the one-step fabrication of actuated devices. The hand contains 18 GRACEs of different sizes and types: fourteen 20-mm-long GRACE-Cs in

the hand palm and four 30-mm-long GRACE-As in the wrist. Each finger can move independently through a tendon controlled by three (two for the thumb) GRACE-Cs in series (Fig. 5A). The wrist consists of four GRACE-As constrained by a compliant joint and showcases the antagonistic operation of the GRACEs. For instance, contracting two adjacent actuators and extending the other two make the wrist deviate, flex, and extend (Fig. 5, B and C; figs. S21 and S22; and movie S6). Each finger joint reaches a bending angle of around 25° whereas the wrist achieves ±15° and ±30° bending around the axis perpendicular and parallel to the hand palm, respectively. The richness of movements of the monolithic GRACE hand (Fig. 5, D and E, and movie S7) gives a hint of the range of biomimetic movements that could be achieved thanks to the versatility of the GRACEs. It also demonstrates that the GRACEs can make the development of functional devices and prototypes that require such actuators accessible to anyone with a desktop 3D printer.
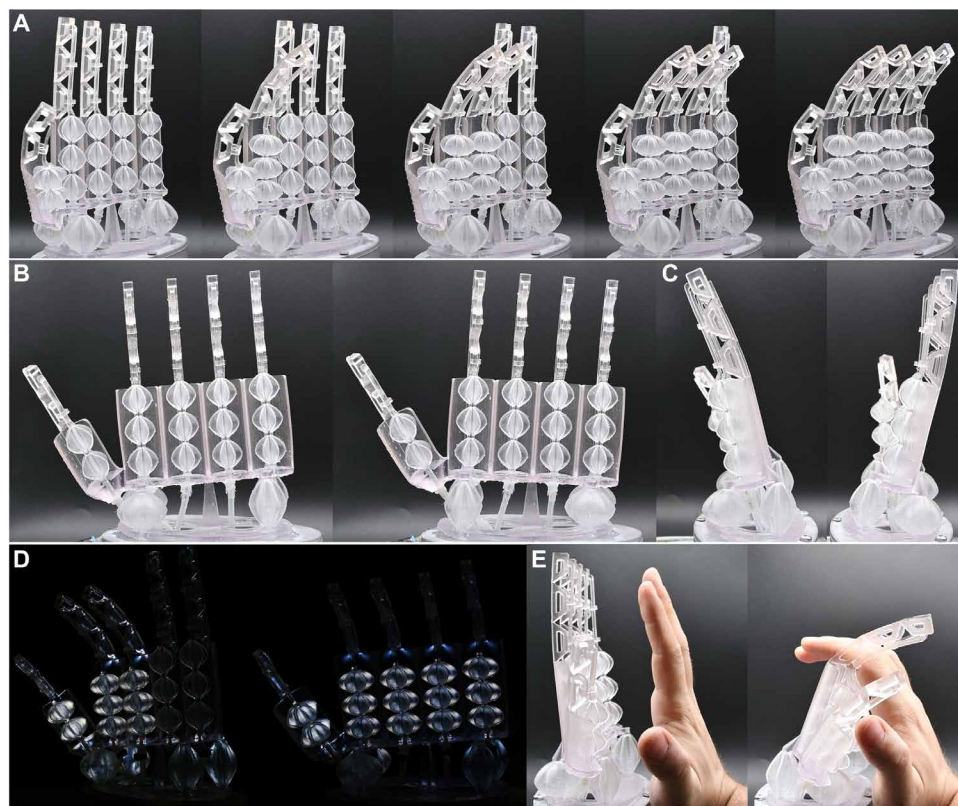
Fig. 5. GRACE-based "pneumatic robotic hand." (**A**) Fingers at rest and actuated whereas the wrist is at rest. (**B** and **C**) Rotational movements enabled by the bidirectional bending of the wrist. (**D**) Actuation of the embodied GRACEs highlighted by photoelasticity. (**E**) Lifelike movement of the GRACE hand.

DISCUSSION

Our results demonstrate that the GRACEs are an extremely versatile and easily fabricated class of PAMs. The GRACEs have overall performances akin to those of state-of-the-art PAMs (table S3), yet they show a substantially higher level of versatility. Their actuation behavior can be tuned at will, they can be scaled within a wide range of size, and their actuation strength can be changed substantially. On the basis of each specific application of the GRACEs, it is possible to define the best design considering the required performance and size constraints. The puffy shape of the GRACEs, which is shared by all designs generated with the model, makes them apparently bulkier than other PAMs of the same length and may represent a problem in some applications where compactness is crucial. This, however, can be easily overcome by scaling down and arranging several GRACEs in series, without increasing the manufacturing effort (as we did in the hand palm for actuating the fingers). The monolithic design of the GRACEs enables the direct 3D-printing of artificial muscles and functional pneumatic devices in one step. The GRACEs, therefore, enable the realization of complex actuated structures with smooth movements that mimic those of animals and humans. Moreover, the GRACEs' development process—consisting of modeling, FEA-based refinement, and additive manufacturing steps—is amenable to automated mass customization, allowing for the straightforward production of different GRACEs on demand (fig. S18). During both the characterization and the 1000-cycle test, we experienced no specific weaknesses related to their structure. However, the contraction force is limited by the adhesion strength between the layers in samples fabricated by fused deposition modeling (FDM). This might be overcome by arranging multiple GRACEs in parallel. In the future, more in-depth studies on their actuation performance depending on different materials and additive manufacturing processes should be carried out. In future work, we will exploit the GRACEs to mimic the large variety of muscle arrangements present in the animal kingdom with the aim of realizing bioinspired machines.

MATERIALS AND METHODS
GRACE design and finite element models

The GRACE designs were carried out using SolidWorks CAD software, and the finite element method simulations were performed by importing the corresponding .stl files into ANSYS Workbench software. Through static structural analysis accounting for large displacements, we simulated the behaviors of the three representative GRACE designs, refined their wall thicknesses to reduce local stress concentrations, and predicted the forces exerted for different material properties. All materials were modeled with a linear elastic behavior whose properties (secant Young's Modulus and Poisson ratio) were extrapolated from the corresponding datasheets. We set the Poisson ratio equal to 0.4 for all the thermoplastic polyurethane and elastomer materials and resins we simulated. For the Flexible 80A resin (Formlabs), we set 5 MPa Young's modulus, 6 MPa for the FlexMark 7 (Treed Filaments), 10 MPa for the FlexMark 8 (Treed Filaments), 12 MPa for the NinjaFlex (NinjaTek), 30 MPa for the FilaFlexible40 (FilaTech), 33 MPa for the Flexfill TPU 92A (Fillamentum), 35 MPa for the FlexMark 9 (Treed Filaments), and 46 MPa for the Flexfill TPU 98A (Fillamentum). The meshes involved tetrahedral elements of 0.5-mm main dimension and were built using the cyclic symmetrical property of the designs starting from one pleat. We used two different sets of boundary conditions for the simulations: one end of the GRACE muscle fixed and the other end free with an applied constant load to reproduce the isotonic conditions, and one end of the GRACE muscle fixed and the other end stretched with a constant displacement to reproduce the isometric conditions. The pressure inputs were applied as a linear function of time with 10 steps.

GRACEs and pneumatic hand fabrication

To realize GRACE samples, we adopted several commercial materials through two additive manufacturing techniques, FDM and SLA. For FDM, we used the i3 MK3S 3D printer by Prusa, and for the SLA, we used both Form 2 and Form 3 by Formlabs. For the manufacturing with the Prusa 3D printer, we used NinjaFlex (Shore Hardness 85A) filaments by NinjaTek, FlexMark 7-8-9 (Shore Hardness 70A, 81A,

93A) by Treed Filaments, FlexFill TPU (Shore Hardness 92A, 98A) by Fillamentum, and FilaFlexible40 (Shore Hardness 40D) by FilaTech, whereas two different versions of the same photopolymer resin—Flexible v2 (85A) and the Flexible 80A, both by Formlabs—were used for the Form 2.

To fabricate the samples for the characterization and the pneumatic hand (fig. S19), we chose SLA-based 3D printing (Formlabs Form 2 and Form 3) because of both high resolution and wide range of printable structure sizes, but other desktop 3D printers can be used as well.

Isotonic and isometric tests

To characterize the GRACEs, we carried out three isotonic (0, 4, and 8 N) and three isometric tests (0, 4, and 8 mm) for each of the three main designs, doubled in the case of the antagonistic design for contraction and extension, for a total of 24 tests. For each test, we used five samples. The samples were held in a Zwick/Roell Z005 testing machine with a 50-N load cell to record the displacement and the force (fig. S17). Through the testing machine, we applied and maintained constant stretching forces during isotonic tests and stretching displacements during isometric tests. The samples were pressurized by a compressor and depressurized by a vacuum pump connected, respectively, to a pressure regulator and a vacuum regulator, both controlled by a wave generator. The overpressure was measured with a pressure sensor and the de-pressure was measured by a vacuum sensor, both connected to a National Instrument board. For each test, we applied five cycles of trapezoidal wave voltage input from the wave generator to the regulators to generate a trapezoidal wave of pressure with five cycles. We set different length time parameters for the wave of the isotonic tests and the isometric ones. Their lengths were chosen after having determined the characteristic time constants of the viscoelastic behavior of the material by previous creep and stress relaxation tests on dog bone samples. In this way, there was enough time between the cycles to allow the sample to return to its starting condition (relaxation time >5 corresponding characteristic times, 5 min for isotonic tests, and 3 min for isometric tests) and to ensure that the actuation time was short enough to avoid high viscoelastic behaviors (each cycle ramp <1 corresponding characteristic time, 1 min for isotonic tests, and 30 s for isometric tests).

Photoelasticity test

The experimental setup is shown (fig. S23). The linear polarized light emitted from the liquid crystal display (LCD) screen passed through the GRACE sample or the pneumatic hand. A linear polarizer film that was crossed with respect to the transmission orientation of the LCD was adopted as analyzer and a camera was used to capture the resulting color map.

One thousand–cycle test and dynamical test

In the 1000-cycle tests, we used the same setup as for the characterization tests but with different inputs to the regulators. The inputs were triangular waves without relaxing time between each cycle with a period of 30 s (15 s each ramp). As for the isotonic test with no load applied, the testing machine was involved only to record the displacement while keeping the force applied null. In the dynamical test, we replaced the testing machine with the Aurora magnetic tracking system (Northern Digital Inc.), which was better able to follow higher-frequency deformations. We applied triangular wave

inputs as for the 1000-cycle test but with frequencies spanning from 0.066 to 1 Hz.

3D-printed artificial hand setup

To actuate the artificial hand with automated sequences of motion, we built a dedicated pneumatic circuit (fig. S20) and controlled the electro-valves through an Arduino Mega board. For the GRACE-C embedded in the five fingers, we used five 2/2 electro-valves, one for each finger, and one overpressure regulator. For the four GRACE-A of the wrist, we used four 3/2 electro-valves to switch from pressurization to depressurization, four 2/2 electro-valves to open and close the inlet inputs, one overpressure regulator, and one vacuum regulator. Each finger was actuated with pressure inputs of 20 kPa, whereas 16 kPa input was adopted for the contracting GRACE-As and −8 kPa input was adopted for the actively elongating ones.

REFERENCES AND NOTES

1. A. A. Biewener, Biomechanics of mammalian terrestrial locomotion. *Science* **250**, 1097–1103 (1990).
2. M. H. Dickinson, C. T. Farley, R. J. Full, M. A. R. Koehl, R. Kram, S. Lehman, How animals move: An integrative view. *Science* **288**, 100–106 (2000).
3. I. W. Hunter, S. Lafontaine, A comparison of muscle with artificial actuators. *Tech. Dig. IEEE Solid-State Sens. Actuator Work.* , 178–185 (1992).
4. J. D. Madden, N. Vandesteeg, P. A. Anquetil, P. G. Madden, A. Takshi, Z. Rachel, S. R. Lafontaine, P. A. Wieringa, I. W. Hunter, Artificial muscle technology: Physical principles and naval prospects. *IEEE J. Ocean. Eng.* **29**, 706–728 (2004).
5. J. Kim, J. W. Kim, H. C. Kim, L. Zhai, H. U. Ko, R. M. Muthoka, Review of soft actuator materials. *Int. J. Precis. Eng. Manuf.* **20**, 2221–2241 (2019).
6. A. Miriyev, A focus on soft actuation. *Actuators* **8**, 74 (2019).
7. E. Acome, S. K. Mitchell, T. G. Morrissey, M. B. Emmett, C. Benjamin, M. King, M. Radakovitz, C. Keplinger, Hydraulically amplified self-healing electrostatic actuators with muscle-like performance. *Science* **359**, 61–65 (2018).
8. H. Wang, P. York, Y. Chen, S. Russo, T. Ranzani, C. Walsh, R. J. Wood, Biologically inspired electrostatic artificial muscles for insect-sized robots. *Int. J. Rob. Res.* **40**, 895–922 (2021).
9. D. Yang, M. S. Verma, J. H. So, B. Mosadegh, C. Keplinger, B. Lee, F. Khashai, E. Lossner, Z. Suo, G. M. Whitesides, Buckling pneumatic linear actuators inspired by muscle. *Adv. Mater. Technol.* **1**, 31–33 (2016).
10. G. K. Klute, J. M. Czerniecki, B. Hannaford, McKibben artificial muscles: Pneumatic actuators with biomechanical intelligence, in *IEEE/ASME Int. Conf. Adv. Intell. Mechatronics, AIM*, (IEEE, 1999), pp. 221–226.
11. F. Daerden, D. Lefeber, B. Verrelst, R. Van Ham, Pleated pneumatic artificial muscles: Actuators for automation and robotics, in *IEEE/ASME Int. Conf. Adv. Intell. Mechatronics, AIM* (IEEE, 2001), vol. 4, pp. 738–743.
12. S. Krishna, T. Nagarajan, A. M. A. Rani, Review of current development of pneumatic artificial muscle. *J. Appl. Sci.* **11**, 1749–1755 (2011).
13. G. Andrikopoulos, G. Nikolakopoulos, S. Manesis, A survey on applications of pneumatic artificial muscles, in *2011 19th Mediterr. Conf. Control Autom. MED 2011*, (IEEE, 2011), pp. 1439–1446.
14. S. Terryn, J. Brancart, D. Lefeber, G. Van Assche, B. Vanderborght, Self-healing soft pneumatic robots. *Sci. Robot.* **2**, eaan4268 (2017).
15. F. Daerden, D. Lefeber, Pneumatic artificial muscles: Actuators for robotics and automation. *Eur. J. Mech. Environ. Eng.* **47**, 11–21 (2002).
16. J. Bishop-Moser, S. Kota, Design and modeling of generalized fiber-reinforced pneumatic soft actuators. *IEEE Trans. Robot.* **31**, 536–545 (2015).
17. A. Miriyev, K. Stack, H. Lipson, Soft material for soft actuators. *Nat. Commun.* **8**, 1–8 (2017).
18. D. Rus, M. T. Tolley, Design, fabrication and control of soft robots. *Nature* **521**, 467–475 (2015).
19. D. Trivedi, C. D. Rahn, W. M. Kier, I. D. Walker, Soft robotics: Biological inspiration, state of the art, and future research. *Appl. Bionics Biomech.* **5**, 99–117 (2008).

20. C. Laschi, B. Mazzolai, M. Cianchetti, Soft robotics: Technologies and systems pushing the boundaries of robot abilities. *Sci. Robot.* **1**, eaah3690 (2016).

21. S. Coyle, C. Majidi, P. LeDuc, K. J. Hsia, Bio-inspired soft robotics: Material selection, actuation, and design. *Extrem. Mech. Lett.* **22**, 51–59 (2018).

22. R. S. Diteesawat, T. Helps, M. Taghavi, J. Rossiter, Characteristic analysis and design optimization of bubble artificial muscles. *Soft Robot.* **8**, 186–199 (2021).

23. P. H. Nguyen, W. Zhang, Design and computational modeling of fabric soft pneumatic actuators for wearable assistive devices. *Sci. Rep.* **10**, 1–13 (2020).

24. Y. L. Park, J. Santos, K. G. Galloway, E. C. Goldfield, R. J. Wood, A soft wearable robotic device for active knee motions using flat pneumatic artificial muscles, in *Proc. - IEEE Int. Conf. Robot. Autom.*, (IEEE, 2014), pp. 4805–4810.

25. S. Kurumaya, H. Nabae, G. Endo, K. Suzumori, Design of thin McKibben muscle and multifilament structure. *Sens. Actuator A Phys.* **261**, 66–74 (2017).

26. S. Kurumaya, K. Suzumori, H. Nabae, S. Wakimoto, Musculoskeletal lower-limb robot driven by multifilament muscles. *ROBOMECH J.* **3**, 1–15 (2016).

27. D. R. Higueras-Ruiz, M. W. Shafer, H. P. Feigenbaum, Cavatappi artificial muscles from drawing, twisting, and coiling polymer tubes. *Sci. Robot.* **6**, eabd5383 (2021).

28. T. J. Wallin, J. Pikul, R. F. Shepherd, 3D printing of soft robotic systems. *Nat. Rev. Mater.* **3**, 84–100 (2018).

29. B. N. Peele, T. J. Wallin, H. Zhao, R. F. Shepherd, 3D printing antagonistic systems of artificial muscle using projection stereolithography. *Bioinspir. Biomim.* **10**, 055003 (2015).

30. M. Schaffner, J. A. Faber, L. Pianegonda, P. A. Rühs, F. Coulter, A. R. Studart, 3D printing of robotic soft actuators with programmable bioinspired architectures. *Nat. Commun.* **9**, 878 (2018).

31. F. Daerden, thesis, Vrije Universiteit Brussel (1999).

32. D. Villegas, M. Van Damme, B. Vanderborght, P. Beyl, D. Lefeber, Third-generation pleated pneumatic artificial muscles for robotic applications: Development and comparison with Mckibben muscle. *Adv. Robot.* **26**, 1205–1227 (2012).

Science Robotics

3D-printed biomimetic artificial muscles using soft actuators that contract and elongate

Corrado De Pascali, Giovanna Adele Naselli, Stefano Palagi, Rob B. N. Scharff, and Barbara Mazzolai

View the article online
https://www.science.org/doi/10.1126/scirobotics.abn4155
Permissions
https://www.science.org/help/reprints-and-permissions

Use of this article is subject to the Terms of service